

# The Role of Groups in Galaxy Evolution: compelling evidence of pre-processing out to the turnaround radius of clusters

Paulo A. A. Lopes,<sup>1\*</sup>, André L. B. Ribeiro<sup>2</sup>, Douglas Brambila<sup>1</sup>

<sup>1</sup>*Observatório do Valongo, Universidade Federal do Rio de Janeiro, Ladeira do Pedro Antônio 43, Rio de Janeiro, RJ, 20080-090, Brazil*

<sup>2</sup>*Laboratório de Astrofísica Teórica e Observacional – Departamento de Ciências Exatas e Tecnológicas – Universidade Estadual de Santa Cruz, 45650-000, Ilhéus, BA, Brazil*

Accepted XXX. Received YYY; in original form ZZZ

## ABSTRACT

We present clear and direct evidence of the pre-processing effect of group galaxies falling into clusters in the local Universe ( $z \lesssim 0.1$ ). We start with a sample of 238 clusters, from which we select 153 with  $N_{200} \geq 20$ . We considered 1641 groups within the turnaround radius ( $\sim 5 \times R_{200}$ ) of these 153 clusters. There are 6654 *individual cluster galaxies* and 4133 *group galaxies* within this radius. We considered two control samples of galaxies, in isolated groups and in the field. The first comprises 2601 galaxies within 1606 *isolated groups*, and the latter has 4273 field objects. The fraction of star forming galaxies in infalling groups has a distinct clustercentric behavior in comparison to the remaining cluster galaxies. Even at  $5 \times R_{200}$  the *group galaxies* already show a reduced fraction of star forming objects. At this radius, the results for the *individual cluster galaxies* is actually compatible to the field. That is strong evidence that the group environment is effective to quench the star formation prior to the cluster arrival. The group star forming fraction remains roughly constant inwards, decreasing significantly only within the cluster  $R_{200}$  radius. We have also found that the pre-processing effect depends on the group mass (indicated by the number of members). The effect is larger for more massive groups. However, it is significant even for pairs and triplets. Finally, we find evidence that the time scale required for morphological transformation is larger than the one for quenching.

**Key words:** surveys – galaxies: clusters: general – galaxies: groups: general – galaxies: star formation – galaxies: evolution.

## 1 INTRODUCTION

According to the concordance model of the Universe ( $\Lambda$ CDM) low-mass dark matter halos are formed first (at high redshift), while larger halos come later through mergers and/or accretion of smaller systems. In this hierarchical structure formation scenario galaxy clusters represent the most massive and latest systems to form in the Universe due to their own gravity. Hence, we expect the presence of substructures, in the form of infalling groups, within clusters. That has been detected for many years, in different wavelengths (Bahcall 1977; Jones & Forman 1984; Dressler & Shectman 1988; Mohr et al. 1993; Pinkney et al. 1996; Girardi et al. 1997; Lopes et al. 2006, 2018).

Galaxy properties are well known to depend on the environment they are located (Oemler 1974; Dressler 1980; Baldry et al. 2006; Cucciati et al. 2006; Cooper et al. 2006). Late-type, gas rich, blue star forming galaxies prefer sparse populated regions of the Universe, while early-type, gas poor, red passive objects dominate the most dense locations, such as the central parts of groups and clusters. Several mechanisms are expected to influence galaxy evolution in dense environments. Those processes can be related to interactions to other members and/or the cluster potential. Another possibility is through interactions with the hot gas trapped in massive systems

(groups and clusters, De Lucia et al. 2012). However, some mechanisms (such as tidal and ram pressure stripping) are more effective in the central parts of clusters, while some are more common in their outskirts and within groups. For example, due to the high relative velocity between cluster members, mergers are a rare phenomenon within their virial radius, being more common inside groups.

The combination of the hierarchical structure growth with the environment dependence of galaxy properties naturally creates the expectation that part of galaxies within clusters (those infalling within groups) are more evolved than the remaining. This fast aging is a result of their prior life within the dense environment of a group. The term used to describe this phenomenon is 'pre-processing' (Zabludoff et al. 1996; Fujita 2004). This process has been extensively investigated in the past years, using simulations (Bahé et al. 2019; Han et al. 2018; Bakels et al. 2021) and/or observations (Cortese et al. 2006; Dressler et al. 2013; Roberts & Parker 2017; Einasto et al. 2020; Estrada et al. 2023). It can be detected through the investigation of many different properties. For instance, it has been shown that the fraction of star forming (SF) galaxies in clusters increases from the center to the outskirts, but never reaching the field level (even at very large radius). The interpretation is that galaxies arriving in clusters, but previously belonging to groups, had their evolution accelerated in the group environment, leading to a reduced fraction of SF objects among those systems (Lewis et al. 2002; Haines et al. 2015; Bianconi

\* E-mail: plopes@ov.ufrj.br

et al. 2018). The existence of merging features among some cluster galaxies is also taken as an indirect proof of the pre-processing effect, as mergers are much more likely to happen within groups. It is important to bear in mind that galaxies arriving in clusters within groups will also face what is called *post-processing*, a combination of the environmental effects from the parent group and the cluster. However, it is difficult to disentangle this effect, which has not been deeply investigated (an exception is found in Choque-Challapa et al. 2019).

Previous studies in the literature have focused on different aspects of the pre-processing effect. For instance, McGee et al. (2009); De Lucia et al. (2012); Bahé et al. (2013); Pallero et al. (2019) investigated the accretion history of group galaxies into clusters. Donnari et al. (2021) aimed to disentangle the effects of AGN feedback, environment, and pre-processing, finding those depend on the galaxy and host mass. Some works investigated the variation of the star-forming (or passive) population as a function of clustercentric distance (Haines et al. 2015). However, just a few studies tried to separate the group from the non-group populations (Hou et al. 2014; Bianconi et al. 2018) and sampled clusters down to at least  $5 \times R_{200}$  (Lewis et al. 2002).

This letter presents an investigation of the pre-processing effect (focusing on the variation of the star formation and late-type fractions), based on a large sample of cluster galaxies, which are separated in galaxies belonging or not to infalling groups, up to the turnaround radius. We have also used two control samples of galaxies, in isolated groups and in the field, for comparison.

This work is structured as follows. In Section 2 we described our data and methodology to build each sample. In §3 we present our results, while a discussion is made in §4. The cosmology assumed in this work considers  $\Omega_m = 0.3$ ,  $\Omega_\lambda = 0.7$ , and  $H_0 = 100 \text{ h km s}^{-1} \text{ Mpc}^{-1}$ , with  $h$  set to 0.7.

## 2 DATA AND METHODOLOGY

### 2.1 The galaxy data

The photometric and spectroscopic data used in this paper were taken from the seventh release of the Sloan Digital Sky Survey (SDSS). The magnitudes retrieved from the SDSS are de-reddened model magnitudes. We derived absolute magnitudes taking in account the distance modulus,  $k$  and  $e$ -corrections. Rest-frame colours are also derived for all objects. We also use the total stellar mass and star formation rate values (SFRs) obtained by the MPA-JHU group Brinchmann et al. (2004). Note that this study is based only on a complete sample of what we call *bright galaxies*, having  $M_r \leq M^* + 1$  ( $\leq -20.58$ ). We also impose a minimum stellar mass cut ( $\text{Log } M_* = 9.50$ ).

We adopt the  $\Sigma_5$  galaxy density estimator as a tracer of the local environment. For each galaxy in our sample, we compute the projected distance,  $d_5$ , to the 5th nearest galaxy around it. We also impose to the neighbor search a maximum velocity offset of  $1000 \text{ km s}^{-1}$ , and a maximum luminosity, which we adopt as  $M_r = M^* + 1$ . The local density  $\Sigma_5$  is simply given by  $5/\pi d_5^2$ , and is measured in units of galaxies/Mpc<sup>2</sup>. Finally, we also take in account the fiber collision issue when deriving galaxy densities. The procedure is well described in La Barbera et al. (2010); Lopes et al. (2014).

### 2.2 Clusters and groups

This work investigates the properties of galaxies belonging to clusters out to the turnaround radius ( $R_{\text{ta}}$ , assumed to be  $\sim 5 \times R_{200}$ , as shown

in Rines & Diaferio 2006). Some of these galaxies are falling into the clusters as part of other systems (groups), while the remaining comprises the rest of the cluster population (galaxies not associated to any infalling group). For the current work, we call the first population as *group galaxies* and the second as *individual cluster galaxies*. We separate the two populations as we identify which cluster galaxies belong to infalling groups. We describe below the cluster and group samples and the identification of the different galaxy populations.

#### 2.2.1 The cluster sample

The cluster sample is a combination of different catalogs that we have been working with for the past years. We have clusters from the supplement version of the Northern Sky Optical Cluster Survey (NoSOCS, Lopes et al. 2004, 2009), the Cluster Infall Regions in the SDSS (CIRS, Rines & Diaferio 2006), the Highest X-ray FLUX Galaxy Cluster Sample (HIFLUGCS, Reiprich & Böhringer 2002; Andrade-Santos et al. 2017), the Planck Early Sunyaev-Zel’Dovich (ESZ, Planck Collaboration et al. 2011), the SPIDERS catalog (Kirkpatrick et al. 2021) and now we also add clusters from Tempel et al. (2012) (see §2.2.2 below).

In Brambila et al. (2023) we combined all the catalogs above with the exception of the one from Tempel et al. (2012). For the current work we consider only objects with  $0.03 \leq z \leq 0.10$ . The upper redshift limit ( $z = 0.10$ ) is due to the completeness limit of the SDSS main spectroscopic sample, limited at  $r_{\text{petro}} = 17.77$ . That corresponds to an absolute magnitude limit of  $M_r \sim M^* + 1 = -20.58$  at  $z \sim 0.10$ .<sup>1</sup> We consider as clusters all objects with  $M_{200} \geq 10^{14} M_\odot$ . Given these constraints, we have 133 clusters from the above catalogs (without those from Tempel et al. (2012)).

We applied the shifting gapper technique (Fadda et al. 1996; Lopes et al. 2009) to all galaxies with available redshifts around each cluster to select members and exclude interlopers. One difference to our previous approach is to consider all galaxies within  $10.0 \text{ h}^{-1} \text{ Mpc}$  (instead of  $2.5 \text{ h}^{-1} \text{ Mpc}$ ), as we now want to have a member list sampling the infall pattern of the clusters. However, we only use the members within  $2.5 \text{ h}^{-1} \text{ Mpc}$  to derive an initial estimate of the velocity dispersion ( $\sigma_{\text{cl}}$ ). An estimate of  $M_{200}$  is obtained adopting the equation 1 of Ferragamo et al. (2020) (also see Munari et al. 2013). The corrections considered by Ferragamo et al. (2020) to  $\sigma_{\text{cl}}$  and  $M_{200}$  are also employed. Next, an estimate of  $R_{200}$  is derived from the above mass estimate. Then we derive final  $\sigma_{\text{cl}}$  and mass estimates, now considering only members within  $R_{200}$  (instead of  $2.5 \text{ h}^{-1} \text{ Mpc}$ ). We refer the reader to Lopes et al. (2009, 2014, 2018) and Ferragamo et al. (2020) for more details on the estimates above.

This same procedure is applied to all systems in the catalog from Tempel et al. (2012), with at least three FoF members and  $0.03 \leq z \leq 0.10$  (17801 objects). We only use the coordinates, redshift, and velocity limits (derived from the FoF members) as input to our code. We are able to obtain estimates of  $\sigma_{\text{cl}}$ ,  $R_{200}$  and  $M_{200}$  for 2854 groups and clusters of Tempel et al. (2012). We then kept only the 189 clusters of this data set ( $M_{200} \geq 10^{14} M_\odot$ ).

Our original sample described above has 120 clusters (out of 133) within the main contiguous area of SDSS, which is used by Tempel et al. (2012) (see their Fig. 1). Hence, we combined these 120 clusters from our original list to the 189 from Tempel et al. (2012), resulting in 238 objects. We still impose a final cut requiring a minimum number

<sup>1</sup> Note those are the cluster redshift limits. The galaxies within clusters obviously span a slightly broader range ( $0.025 < z < 0.105$ ).

of 20 galaxies within  $R_{200}$  to call an object as a cluster ( $N_{200} \geq 20$ ), leading to a final cluster sample of 153 systems.

There are 17839 *individual galaxies* associated to the 238 clusters described above. Considering only clusters with  $N_{200} \geq 20$  and galaxies within  $5 \times R_{200}$  we are left with 12628 galaxies within the 153 clusters. We actually only work with *bright galaxies* ( $M_r \leq M^* + 1$ ), and impose that  $\text{Log } M_* \geq 9.50$ , so that the final sample comprises 6654 cluster galaxies. A very important remark is that these numbers do not represent the actual number of members obtained by the shifting gapper method. The reason is that we actually excluded from this cluster member list galaxies that are also members of infalling groups (4133 objects), as described in §2.2.2.1. Hence, the total number of cluster members is larger (10787), as we split those in two populations, of *group galaxies* and *individual cluster galaxies*. The number above (6654) reflects only the second population.

### 2.2.2 The group sample

We adopted the group sample from Tempel et al. (2012), which was built using Sloan Digital Sky Survey (SDSS) Data Release 8 (DR8). In reality, their sample comprises groups and clusters. Their clusters were actually use in combination to the other cluster samples above (see §2.2.1). However, the only group sample we consider for this work is theirs.

The authors applied a modified friends-of-friends (FoF) method with a variable linking length in both directions, eliminating selection effects and achieving high completeness. Their catalog has 77858 groups (and clusters) with two or more members. The number of observed members in each group is called its richness. The authors also provide other group parameters that scale with mass, such as an estimate of the virial radius (given by the the projected harmonic mean), the velocity dispersion and total luminosity of the group in the  $r$ -band. Further details on the generation of their catalog with the FoF algorithm, and the available galaxy and group properties, can be found in Tempel et al. (2012).

There are 40330 objects in the catalog from Tempel et al. (2012), with  $0.03 \leq z \leq 0.10$ . In order to eliminate common clusters to our list with 238 clusters described above (in §2.2.1), we compared the two catalogs, keeping 40100 systems with at least two members from Tempel et al. (2012). Those objects have no counterpart to the 238 clusters. For these groups, we kept the FoF membership assignment, which is more appropriate to this very low number of members.

#### 2.2.2.1 The infalling group sample

We considered a membership matching approach to select groups in the infall regions of clusters. We compared all the galaxies that are group members (according to the FoF) to those that are cluster members (from the shifting gapper technique). All the FoF groups with galaxies matched to the cluster member list are considered as infalling groups.

It is obviously possible that not all galaxies from an infalling group have a counterpart among the cluster members. That happens for groups that are close to the escape velocity of a cluster at a given radius. That could be the case for recent arrivals into the clusters or due to imperfect membership assignment (from the FoF or shifting gapper). For those cases, we did consider all group galaxies in our analysis, even if some of them are not matched to cluster galaxies. These objects correspond to  $\sim 12\%$  of the group galaxies. However, we verified that our results (§3) are not affected if we exclude them.

It is important to keep in mind that what we consider as groups infalling into clusters are systems located within the caustic profile

associated to the cluster members. This profile can be seen as the result of the membership selection produced with the shifting gapper technique. Although we have infalling groups with small cluster-centric distances ( $\lesssim R_{200}$ ), their velocity offset distribution (relative to their parent clusters) is non-Gaussian, as expected from an infalling population. That is in full agreement with Haines et al. (2018), who selected infalling X-ray groups around massive clusters. Due to the limited field of view their selection resulted only in groups with small radial offsets ( $0.3 \lesssim R/R_{200} \lesssim 1.3$ ), but with a non-Gaussian velocity distribution.

We find 3792 groups in the infall regions of clusters. However, as we consider the infall region limited to the turnaround radius ( $\sim 5 \times R_{200}$ ) we actually have 1941 groups within this limit, being 1641 groups associated to clusters with  $N_{200} \geq 20$ .

There are 18340 galaxies in the 3792 infalling groups. Considering only groups that are in the infall of clusters with  $N_{200} \geq 20$ , we have 15240 galaxies, from which 7477 are within  $5 \times R_{200}$  of their parent cluster. Out of those we have 4133 bright galaxies (also having  $\text{Log } M_* \geq 9.50$ ). Those are the members of our infalling group sample of 1641 systems.

#### 2.2.2.2 The isolated group sample

We have also created a sample of isolated groups. We did so to have a comparison group sample free of the effects related to the cluster environment. We have 36308 groups that are not in the infall patterns of clusters (after excluding the 3792 infalling groups from the sample of 40100 groups). To consider a group as isolated we do the following. We compare each group to high density galaxies ( $\Sigma_5 \geq 5 \text{ gals/Mpc}^2$ ; typical for galaxies within  $R_{200}$  of clusters). A group is considered isolated if it is not found within 15 Mpc and  $\pm 3000 \text{ km s}^{-1}$  from a high density galaxy. From the 36308 groups we selected 1606 isolated groups. There are 4097 galaxies within those systems, from which 2601 are bright galaxies with  $\text{Log } M_* \geq 9.50$ .

### 2.3 The field sample

One way to characterize the pre-processing effect is through the comparison of the fraction of star forming galaxies (or other populations or galaxy properties) in clusters and in the field. We built a field sample through the comparison of each galaxy (from SDSS DR7) to a group and cluster catalog, as in Brambila et al. (2023). However, here we discard galaxies with a distance smaller than 4 Mpc and with  $|\Delta z| \leq 0.10$  of any object from a combined cluster catalogue (based on the sample from Gal et al. 2009 and all catalogues described above). Besides that, we also avoided galaxies within a radius of 2.0 Mpc and velocity difference of  $\pm 2000 \text{ km s}^{-1}$  from a bright neighbor ( $M_r \leq M^* + 1$ ) in the spectroscopic main sample of the SDSS DR7. We found 4598 bright field galaxies in the same redshift range of cluster galaxies ( $0.025 < z < 0.105$ ). The distribution of  $\text{LOG } \Sigma_5$  shows a sharp cut at -0.5. However, there are still some galaxies ( $< 0.5\%$ ) with larger density values, which we exclude. We also remove one galaxy with  $\text{LOG } \Sigma_5 = -4.0$ . Hence, the field list was then reduced to 4551 bright galaxies (also having  $\text{Log } M_* \geq 9.50$ ). We performed a last cleaning, discarding 278 objects that were part of a group from Tempel et al. (2012), so that the final field sample comprises 4273 bright galaxies. However, the exclusion of these objects do not impact the field results shown below.

To sum up, unless otherwise stated, those are the numbers of bright and massive galaxies ( $M_r \leq M^* + 1$ ;  $\text{Log } M_* \geq 9.50$ ) this work is based on: 6654 (*individual cluster galaxies*), 4133 (*group galaxies*), 2601 (*isolated group galaxies*) and 4273 field objects. The median

values of  $\text{Log } M_*$  (the first and third quartiles are in parenthesis) for these four samples are 10.66 (10.48; 10.87), 10.65 (10.45; 10.87), 10.64 (10.43; 10.87) and 10.54 (10.33; 10.76), respectively.

### 3 PRE-PROCESSING GALAXIES IN GROUPS

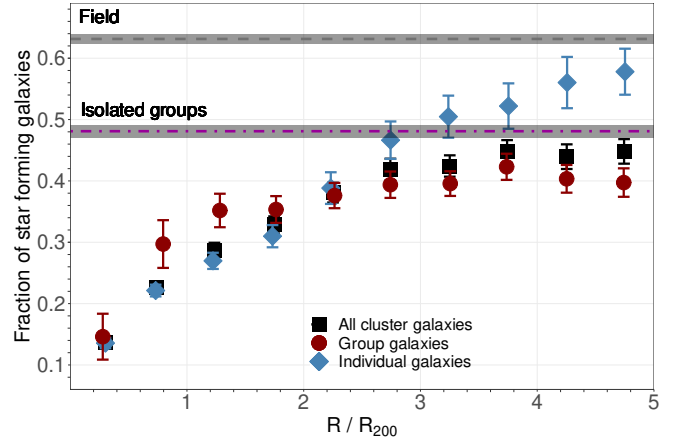
The pre-processing effect is usually characterized in the literature by the difference in the fraction of star forming galaxies ( $F_{\text{SF}}$ ) in clusters and the field. We expect that the  $F_{\text{SF}}$  in clusters to increase from the center to the outskirts of clusters. However, the measurements of  $F_{\text{SF}}$  are generally found to be below the field results, even at large cluster radius ( $\gtrsim 3 \times R_{200}$ , Haines et al. 2015). This difference is interpreted as the result of the group environment affecting cluster galaxies prior to their infall.

In Fig. 1 we display the  $F_{\text{SF}}$  as a function of clustercentric distance (up to  $5 \times R_{200}$ ) for different populations. We consider the galaxy location in the star formation rate-stellar mass plane to classify galaxies as passive or star-forming. We call galaxies as SF if their  $\log(\text{SFR})$  value is greater or equal the line defined by equation 2 of Trussler et al. (2020) ( $\log \text{SFR} = 0.70 \log M_* - 8.02$ ). In Fig. 1 the black squares represent all galaxies that are cluster members and the gray dashed line indicates the field fraction. That is usually what we see in the literature (although observational results normally do not reach  $5 \times R_{200}$ ), being the difference between field and clusters at large radii associated to the pre-processing effect. Here we further separate the cluster data in two subpopulations, of *individual cluster galaxies* (blue diamonds) and *group galaxies* (red circles); see §2.2.1 and §2.2.2.1. We also show the results for galaxies in isolated groups (magenta dot-dashed line).

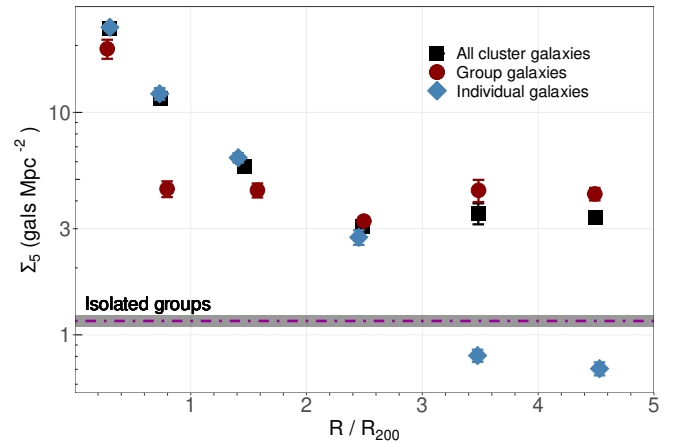
In addition to the usual indirect signature of the pre-processing effect (difference between the field and cluster results - gray line and black points) we now provide direct and compelling evidence in its favor. The  $F_{\text{SF}}$  grows from the center to the clusters' outskirts. However, the blue diamonds (*individual cluster galaxies*) do not display a flat behavior for  $R \gtrsim 2 \times R_{200}$ . Actually, the  $F_{\text{SF}}$  values of *individual cluster galaxies* are reconciled to the field fractions at  $\sim 5 \times R_{200}$ . The difference between the field and cluster results can be fully attributed to the *group galaxies* (red points), as those are previously pre-processed in these dense environments.

Fig. 2 provides a natural explanation for the pre-processing effect. We display the local density parameter ( $\Sigma_5$ ) vs ( $R / R_{200}$ ) for all galaxies in clusters (black squares), *individual cluster galaxies* (blue diamonds) and *group galaxies* (red circles). We also show the results for the isolated groups (magenta dot-dashed line). The mean  $\Sigma_5$  value for the field is  $0.082 \text{ gals Mpc}^{-2}$ . We omit it from the figure for clarity.  $\Sigma_5$  decreases from the central part of clusters to their outskirts. However, the *individual cluster galaxies* (blue points) reach much smaller densities (as they are not part of smaller systems), of  $\sim 0.7 \text{ gals Mpc}^{-2}$ . For  $R \gtrsim 3 \times R_{200}$  the local density ( $\Sigma_5$ ) becomes approximately flat, while the values for the *group galaxies* (red points) reach a plateau for  $R \gtrsim 1 - 2 \times R_{200}$ , with  $\Sigma_5 \sim 4 \text{ gals Mpc}^{-2}$ , reflecting the higher density environment of groups. Hence, this plot, in combination with Fig. 1, confirms that *group galaxies* are quenched before the rest of the cluster population (*individual cluster galaxies*), due to environmental effects within infalling groups.

In Fig. 3 we investigate the possible dependence of the pre-processing effect on group mass, traced by the number of members. The results for pair and triplets ( $N \leq 3$ ) are shown by the red points. The blue points display the fractions for objects with  $3 < N \leq 10$ , while we show in dark gray the results for groups with  $N > 10$ . The results for the field (gray dashed line) and isolated groups (magenta



**Figure 1.** Fraction of star forming galaxies in clusters out to  $5 \times R_{200}$ . Galaxies that are not associated to groups are displayed in blue diamonds, while those that are members of infalling groups are shown in red circles. The fractions for all cluster galaxies (part of groups or not) are in black squares. The field fraction is shown by the gray dashed line, and the fraction for the isolated groups is displayed by the dot-dashed magenta line.  $F_{\text{SF}}$  is computed in intervals of  $0.5 \times (R / R_{200})$ , with the values in the X coordinate given by the mean of all points within each interval. The error bars, and the gray bands over the two horizontal lines, indicate the  $1 \sigma$  standard error of a proportion.



**Figure 2.** The correlation of local galaxy density with normalized clustercentric distance ( $R / R_{200}$ ). The colors of the symbols and lines are the same as for Fig. 1.  $\Sigma_5$  is computed in intervals of  $1.0 \times (R / R_{200})$ , with the values in the X coordinate given by the mean of all points within each interval. The exception is for the first two points (of each population) for which we consider intervals of  $0.5 \times (R / R_{200})$ . The error bars (and the gray band over the horizontal line) indicate the  $1 \sigma$  standard error.

dot-dashed line) are displayed as before. For the first subset ( $N \leq 3$ ) we detect a flat behavior from the outskirts down to  $\sim 2 \times R_{200}$ , with smaller fractions in the two inner bins. The second subset ( $3 < N \leq 10$ ) displays a nearly flat behavior for the whole interval. The results for the most rich groups ( $N > 10$ ) smoothly decrease towards the center (down to  $R \sim 1 \times R_{200}$ ), but within  $R_{200}$ ,  $F_{\text{SF}}$  displays a steep drop. An important result is that at large radii ( $R \gtrsim 2 \times R_{200}$ ) there is a significant difference in the  $F_{\text{SF}}$  values according to the number of members. That indicates the fraction of quenched galaxies is already higher in large groups (in comparison to the smaller systems) when

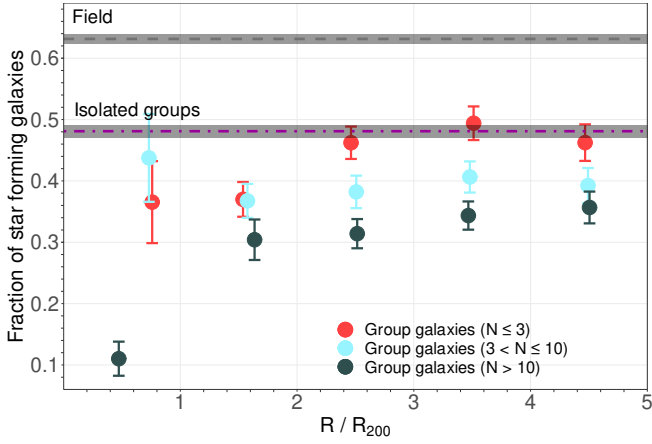


**Figure 3.** Fraction of star forming galaxies vs normalized clustercentric distance ( $R / R_{200}$ ) for galaxies within infalling groups. The results are divided according to the number of the members of the groups. Red points indicate the results for pairs and triplets ( $N \leq 3$ ), while the blue points represent systems with  $3 < N \leq 10$ , and dark gray points are for the most rich objects (with  $N > 10$ ). The lines are the same as for Fig. 1.  $F_{SF}$  is computed in intervals of  $1.0 \times (R / R_{200})$ , with the values in the X coordinate given by the mean of all points within each interval. The error bars (and the gray bands over the two horizontal lines) indicate the  $1\sigma$  standard error of a proportion.

they arrive at the clusters. However, the pre-processing effect is detected even for pairs and triplets, as their  $F_{SF}$  values are smaller than the field expectations.

The different clustercentric dependence, for the *group galaxies* and *individual cluster galaxies*, of  $F_{SF}$  and  $\Sigma_5$ , is also seen for several structural and star formation related galaxy properties. For instance, similar results are found for galaxy specific star formation rate, color, size, concentration, T-type (a number assigned to each type of galaxy, which relates to the Hubble morphological sequence) and fraction of late-type (or early-type) galaxies. Those results reinforce the pre-processing effect and will be extensively discussed in a future paper. Here we show some results regarding morphology in Fig. 4. To classify galaxies as early or late-type (LT) we consider the T-type values and probabilities derived by Domínguez Sánchez et al. (2018). We adopted the criteria described in Brambila et al. (2023) (LT galaxies have  $T\text{-type} > 0$ ,  $P_{S0,bulge} < 0.6$  and  $P_{disc} > 0.8$ ). We can see from Fig. 4 the fraction of late-type galaxies ( $F_{LT}$ ) displays a similar behavior to  $F_{SF}$  as function of ( $R / R_{200}$ ), corroborating the pre-processing in groups. The *group galaxies* have smaller values of  $F_{LT}$  at large clustercentric distances, when compared to the *individual cluster galaxies*. However, an important result we achieve is the fact that the typical values of  $F_{LT}$  are higher than  $F_{SF}$ , for both galaxy populations, suggesting that SF is quenched in a shorter time scale than what is necessary for the morphological transformation to happens (a result we previously showed in Lopes et al. 2014). Note that our results are for bright massive galaxies. The  $F_{LT}$  values at  $R \sim 5 \times R_{200}$  of *individual galaxies* are compatible to their  $F_{SF}$  results. But going inwards  $F_{SF}$  decreases much faster than  $F_{LT}$ .

#### 4 DISCUSSION AND SUMMARY

In this manuscript we present compelling and direct evidence in favor of the pre-processing effect of galaxies within groups. We do so through the comparison of the different populations of cluster

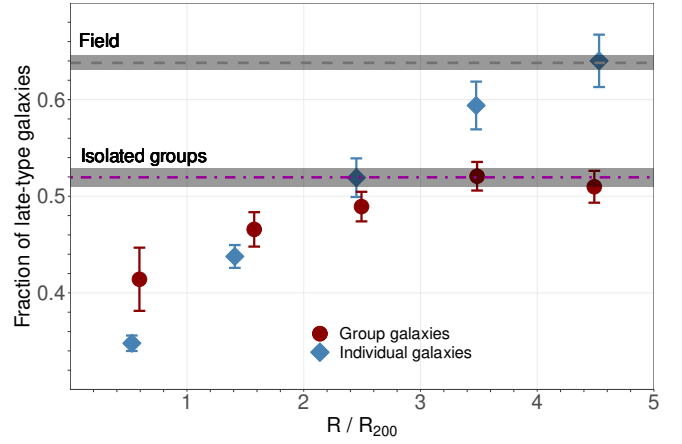


**Figure 4.** Analogous to Fig. 1, but showing the fraction of late-type galaxies. The colors of the symbols and lines are the same as for Fig. 1.  $F_{LT}$  is computed in intervals of  $1.0 \times (R / R_{200})$ , with the values in the X coordinate given by the mean of all points within each interval. The error bars (and the gray bands over the two horizontal lines) indicate the  $1\sigma$  standard error of a proportion.

galaxies, which we named *individual cluster galaxies* (not associated to any subgroup) and *group galaxies* (belonging to subgroups). This approach was tried only a few times in the literature (e.g., Hou et al. 2014; Bianconi et al. 2018). However, it is important to note that previous observational results usually do not reach the turnaround radius ( $\sim 5 \times R_{200}$ ), being limited to at most  $3 \times R_{200}$  (Hou et al. 2014; Haines et al. 2015; Roberts & Parker 2017; Bianconi et al. 2018). An exception is the work of Lewis et al. (2002), but they do not split the cluster galaxies as described above. Some other results in the literature are also restricted to investigate the pre-processing effect in the surrounding regions of a single (or a few) cluster or within a supercluster region (Estrada et al. 2023; Einasto et al. 2020). Our study is based on a large sample of groups (1641 infalling and 1606 isolated) and clusters (153), with the later sampled up to the  $R_{ta}$ . Within this radius we have 6654 *individual cluster galaxies* and 4133 *group galaxies*. Additionally, we have 2601 galaxies within *isolated groups* and 4273 field objects.

The  $F_{SF}$  is measured separately for the two cluster populations all the way out to  $5 \times R_{200}$  (see Fig. 1; to the best of our knowledge that is shown here for the first time). A result first seen here is also the agreement between the cluster  $F_{SF}$  infall (*individual cluster galaxies*) and field values, at large radius (close to the  $R_{ta}$ ). That indicates that *individual galaxies* - when first arriving into clusters - do have similar fractions of star forming objects as in the field. As they travel inwards they are progressively quenched, even at large clustercentric distances (in agreement with Bahé et al. 2013). On the contrary, the *group galaxies* arrive into the clusters with an already reduced fraction of star forming galaxies. Their  $F_{SF}$  values are nearly constant inwards, down to  $\sim 1 - 2 \times R_{200}$ . A significant reduction is found only within  $R_{200}$  (see the red points in Fig. 1).

An interesting result is that at  $\sim R_{200}$  the  $F_{SF}$  of *group galaxies* becomes larger than the ones for the *individual cluster galaxies*. That is in disagreement with Bianconi et al. (2018), who found comparable results within  $R_{200}$ . We interpret this inversion on the behavior of the two populations (when going inside  $R_{200}$ ) as a combination of two effects. First, the  $F_{SF}$  results for the *individual cluster galaxies* (blue points) are *contaminated* by backplash galaxies (that is expected in a large range around  $R_{200}$ ), objects that already crossed the cluster cores once. Hence, being more affected by the cluster environment in

comparison to the *group galaxies*. The latter are actually not expected to survive as group galaxies after the first cluster passage (Choque-Challapa et al. 2019; Haggag et al. 2023), so that the *group galaxies* shown here are probably recent arrivals into the clusters. However, this effect is expected to impact our results as well as the literature ones. Second, and most importantly, the results of Fig. 1 consider all groups in our sample. As seen in Fig. 3 the  $F_{SF}$  depends on the group mass (indicated by the number of members). Smaller groups ( $N \leq 10$ ) show much higher (especially within  $R_{200}$ ) star forming fractions than the richer systems ( $N > 10$ ). Note the results from Bianconi et al. (2018) should reflect what is expected for more massive systems, as they select groups through its X-ray emission.

We have also shown - perhaps for the first time - that the local galaxy densities ( $\Sigma_5$ , see Fig. 2) of the two cluster populations have clustercentric variations that explain the  $F_{SF}$  radial dependence. The  $\Sigma_5$  values of the *individual cluster galaxies* decrease with radial growth, reaching much smaller values than obtained for the *group galaxies*, for  $R \gtrsim 3 \times R_{200}$ . The pre-processing effect is also verified through the reduced fractions of late-type galaxies in the *group* sample compared to the *individual cluster galaxies*. That is seen in Fig. 4, from which we can also infer that the time scale required for the morphological transformation to be larger than the one for quenching.

We performed a few tests in order to verify the robustness of our conclusions. It is well known that the fraction of galaxy populations (such as star-forming or disc) and galaxy properties (such as color and morphology) are known to be correlated with the environment, but also stellar mass. The different populations investigated in the current work have different mass distributions. In order to check if that could impact our results we built stellar mass matched samples of the galaxies in different data sets. For instance, we verified that the  $F_{SF}$  values of the *group galaxies* do not change significantly when using the stellar mass matched samples (in comparison to the *individual cluster galaxies*), which were built in radial bins. The variation of  $F_{SF}$  looks less flat for  $R > 3 \times R_{200}$ , but it is still compatible to the original one (seen in Fig. 1). The only case the difference is larger than  $1-\sigma$  (but still within  $2-\sigma$ ) is for the last radial bin (close to  $5 \times R_{200}$ ).

We have also investigated if the results change if we consider all galaxies in our original sample of 238 clusters, instead of the sample with 153 clusters (requiring  $N_{200} \geq 20$ ). Another test we applied was to select only galaxies with  $\text{Log } M_* \geq 10.0$  (instead of 9.50). For both cases the  $F_{SF}$  values become a little smaller, in comparison to our original results of Fig. 1, but still in agreement, within the error bars.

The results presented in this study represent direct evidence that *group galaxies* are indeed quenched (and experience morphological transformation) before the rest of the cluster population (*individual cluster galaxies*), as the result of environmental processes within infalling groups. It is not the goal of the present work to investigate which processes are actually responsible for the accelerated quenching of the group galaxies before infall. Those could be related to galaxy encounters, starvation or ram-pressure stripping (in the case of the more massive groups), for instance. Our objective is to provide a careful selection of infalling groups within clusters and to disentangle the cluster population in two subsets: *group galaxies* and *individual cluster galaxies*. This way we are able to perform a detailed analysis of the variation of the  $F_{SF}$  (and other properties) for these populations and to compare those to the results from the field and from an isolated group sample. Our results represent an important benchmark for cluster follow-up studies, out to  $5 \times R_{200}$ , aiming

to investigate the pre-processing effect (e.g., the WEAVE Wide-Field Cluster Survey, Cornwell et al. 2022).

## ACKNOWLEDGEMENTS

P.A.A.L. thanks the support of *Conselho Nacional de Desenvolvimento Científico e Tecnológico* (CNPq), grants 433938/2018-8 and 312460/2021-0 and the *Fundação de Amparo à Pesquisa do Estado do Rio de Janeiro do Rio de Janeiro* (FAPERJ), grant E-26/200.545/2023. ALBR thanks the support of CNPq, grant 316317/2021-7, and Fundação de Amparo à Pesquisa do Estado da Bahia (FAPESB) INFRA PIE 0013/2016. DB acknowledges the *Coordenação de Aperfeiçoamento de Pessoal de Nível Superior* (CAPES) for a PhD fellowship. This research has made use of the SAO/NASA Astrophysics Data System and the SDSS. A list of participating institutions can be obtained from the SDSS Web Site (<http://www.sdss.org/>).

## DATA AVAILABILITY

The galaxy, group and cluster catalogs used in this work are public available. However, we are willing to provide - upon reasonable request - the separate lists we have created.

## REFERENCES

- Andrade-Santos F., et al., 2017, *ApJ*, **843**, 76  
 Bahcall N. A., 1977, *ApJ*, **217**, L77  
 Bahé Y. M., McCarthy I. G., Balogh M. L., Font A. S., 2013, *MNRAS*, **430**, 3017  
 Bahé Y. M., et al., 2019, *MNRAS*, **485**, 2287  
 Bakels L., Ludlow A. D., Power C., 2021, *MNRAS*, **501**, 5948  
 Baldry I. K., Balogh M. L., Bower R. G., Glazebrook K., Nichol R. C., Bamford S. P., Budavari T., 2006, *MNRAS*, **373**, 469  
 Bianconi M., Smith G. P., Haines C. P., McGee S. L., Finoguenov A., Egami E., 2018, *MNRAS*, **473**, L79  
 Brambila D., Lopes P. A. A., Ribeiro A. L. B., Cortesi A., 2023, *MNRAS*, **523**, 785  
 Brinchmann J., Charlot S., White S. D. M., Tremonti C., Kauffmann G., Heckman T., Brinkmann J., 2004, *MNRAS*, **351**, 1151  
 Choque-Challapa N., Smith R., Candlish G., Peletier R., Shin J., 2019, *MNRAS*, **490**, 3654  
 Cooper M. C., et al., 2006, *MNRAS*, **370**, 198  
 Cornwell D. J., et al., 2022, *MNRAS*, **517**, 1678  
 Cortese L., Gavazzi G., Boselli A., Franzetti P., Kennicutt R. C., O’Neil K., Sakai S., 2006, *A&A*, **453**, 847  
 Cucciati O., et al., 2006, *A&A*, **458**, 39  
 De Lucia G., Weinmann S., Poggianti B. M., Aragón-Salamanca A., Zaritsky D., 2012, *MNRAS*, **423**, 1277  
 Domínguez Sánchez H., Huertas-Company M., Bernardi M., Tuccillo D., Fischer J. L., 2018, *MNRAS*, **476**, 3661  
 Donnari M., et al., 2021, *MNRAS*, **500**, 4004  
 Dressler A., 1980, *ApJ*, **236**, 351  
 Dressler A., Shectman S. A., 1988, *AJ*, **95**, 985  
 Dressler A., Oemler Augustus J., Poggianti B. M., Gladders M. D., Abramson L., Vulcani B., 2013, *ApJ*, **770**, 62  
 Einasto M., et al., 2020, *A&A*, **641**, A172  
 Estrada N., et al., 2023, *A&A*, **671**, A146  
 Fadda D., Girardi M., Giuricin G., Mardirossian F., Mezzetti M., 1996, *ApJ*, **473**, 670  
 Ferragamo A., Rubiño-Martín J. A., Betancort-Rijo J., Munari E., Sartoris B., Barrena R., 2020, *A&A*, **641**, A41  
 Fujita Y., 2004, *PASJ*, **56**, 29

- Gal R. R., Lopes P. A. A., de Carvalho R. R., Kohl-Moreira J. L., Capelato H. V., Djorgovski S. G., 2009, *AJ*, **137**, 2981
- Girardi M., Escalera E., Fadda D., Giuricin G., Mardirossian F., Mezzetti M., 1997, *ApJ*, **482**, 41
- Haggar R., Kuchner U., Gray M. E., Pearce F. R., Knebe A., Yepes G., Cui W., 2023, *MNRAS*, **518**, 1316
- Haines C. P., et al., 2015, *ApJ*, **806**, 101
- Haines C. P., et al., 2018, *MNRAS*, **477**, 4931
- Han S., Smith R., Choi H., Cortese L., Catinella B., Contini E., Yi S. K., 2018, *ApJ*, **866**, 78
- Hou A., Parker L. C., Harris W. E., 2014, *MNRAS*, **442**, 406
- Jones C., Forman W., 1984, *ApJ*, **276**, 38
- Kirkpatrick C. C., et al., 2021, *MNRAS*, **503**, 5763
- La Barbera F., Lopes P. A. A., de Carvalho R. R., de La Rosa I. G., Berlind A. A., 2010, *MNRAS*, **408**, 1361
- Lewis I., et al., 2002, *MNRAS*, **334**, 673
- Lopes P. A. A., de Carvalho R. R., Gal R. R., Djorgovski S. G., Odewahn S. C., Mahabal A. A., Brunner R. J., 2004, *AJ*, **128**, 1017
- Lopes P. A. A., de Carvalho R. R., Capelato H. V., Gal R. R., Djorgovski S. G., Brunner R. J., Odewahn S. C., Mahabal A. A., 2006, *ApJ*, **648**, 209
- Lopes P. A. A., de Carvalho R. R., Kohl-Moreira J. L., Jones C., 2009, *MNRAS*, **392**, 135
- Lopes P. A. A., Ribeiro A. L. B., Rembold S. B., 2014, *MNRAS*, **437**, 2430
- Lopes P. A. A., Trevisan M., Laganá T. F., Durret F., Ribeiro A. L. B., Rembold S. B., 2018, *MNRAS*, **478**, 5473
- McGee S. L., Balogh M. L., Bower R. G., Font A. S., McCarthy I. G., 2009, *MNRAS*, **400**, 937
- Mohr J. J., Fabricant D. G., Geller M. J., 1993, *ApJ*, **413**, 492
- Munari E., Biviano A., Borgani S., Murante G., Fabjan D., 2013, *MNRAS*, **430**, 2638
- Oemler Augustus J., 1974, *ApJ*, **194**, 1
- Pallero D., Gómez F. A., Padilla N. D., Torres-Flores S., Demarco R., Cerulo P., Olave-Rojas D., 2019, *MNRAS*, **488**, 847
- Pinkney J., Roettiger K., Burns J. O., Bird C. M., 1996, *ApJS*, **104**, 1
- Planck Collaboration et al., 2011, *A&A*, **536**, A8
- Reiprich T. H., Böhringer H., 2002, *ApJ*, **567**, 716
- Rines K., Diaferio A., 2006, *AJ*, **132**, 1275
- Roberts I. D., Parker L. C., 2017, *MNRAS*, **467**, 3268
- Tempel E., Tago E., Liivamägi L. J., 2012, *A&A*, **540**, A106
- Trussler J., Maiolino R., Maraston C., Peng Y., Thomas D., Goddard D., Lian J., 2020, *MNRAS*, **491**, 5406
- Zabludoff A. I., Zaritsky D., Lin H., Tucker D., Hashimoto Y., Shectman S. A., Oemler A., Kirshner R. P., 1996, *ApJ*, **466**, 104

This paper has been typeset from a  $\text{\TeX}/\text{\LaTeX}$  file prepared by the author.